A NEW CONCEPT OF THE STRUCTURE OF THE POROUS GAS DIFFUSION ELECTRODE

Dr Olle Lindström

Central Laboratories, ASEA, Västerås, Sweden

1. Introduction

The author described the wetted porous fuel cell electrode in 1963 in the following way (1,2): "The reaction zone is assumed to lie in this extended meniscus. The walls in the gas-filled pores in the gas-diffusion electrode are thus covered by a thin film of electrolyte (cf. Fig. 1). The reaction gas is dissolved in the electrolyte film, diffuses to the electrode surface and reacts there so that electrons are taken from, or yielded to, the electrode. The reaction products diffuse away from the reaction site, which is released for a new reaction. The electrolyte film should obviously cover large surfaces in the interior of the porous electrode and stand in good communication with both the gas side and the electrolyte side." - This thin film hypothesis was presented independently by several fuel cell workers at that time. This was quite natural, since it is difficult to conceive that a sharp three-phase boundary could exist in a wetted porous electrode, where the contact angle is almost zero. Will was the first to present experimental evidence of the existence of an electrolyte film in the case of solid, partially immersed electrodes (3,4).

The studies of the gas-diffusion electrode have been dominated by the mathematical treatment of the system of basic equations governing the electrode processes. As a rule, the gas diffusion electrode is then considered to be a population of pores, irrespective of whether the theory utilises the thin-film hypothesis of the hypothesis of a linear three-phase boundary.

The question of structure, however, is the key problem in this connection. The creditable attempts made up to now to give an adequate and effective description of the structure of the porous gas-diffusion electrode on the basis of pore models have not been entirely successful. Ksenzhek admits that attempts to correlate the properties of porous electrodes with the simple pore models have only resulted in greater complexity (5). The porous electrode is therefore conceived by Ksenzhek to be a pseudohomogeneous medium, the properties of which are characterised by effective parameters defining the mass transfer and kinetic properties of the medium. Micka has coined the expression "fine-structure models" (6) for this type of continuous or semi-continuous electrode model, and this has also been utilised by Ksenzhek (5) and Micka in later works as well as by Newman and Tobias (7).

The electrode model presented below is an attempt in another direction. A geometrical model is developed, which corresponds as far as possible to reality. The electrode structure is characterised with the aid of structure parameters having a real physical import. The working electrode is conceived as a compressed powder with the powder grain surfaces covered by a film of electrolyte, cf. (4,5). This theory has previously been called the "powder film theory" (8,9) because of this conception of the electrode.

The cohesive gas phase between powder grains in the porous electrode structure is conceived as being a network of interstices. This initial concept is supplemented by a model of the cohesive film on the grain surfaces, the film network, which is utilised for describing the mass transfer conditions along the electrolyte film. The electrode structure can then be characterised on the basis of these models with the aid of structure parameters, mainly the film area, film perimeter, film thickness, interstice width, interstice tortuosity and film tortuosity. The structure parameters can be determined in a non-electrochemical way by means of dilatometer measurements, film resistance measurements, etc., under actual service conditions. The model therefore forms a good starting point for the formulation of an absolute electrode and fuel-cell theory.

2. Gas penetration into a porous gas-diffusion electrode

Gas-diffusion electrodes are often produced with the help of powder metallurgy by pressing (or rolling) of metallic powder, followed by a sintering process. Pressing gives the electrode plate a certain strength, which is considerably improved during sintering. During sintering, the grains in the contact surfaces become bonded under the influence of surface forces and plastic deformation. The structure developed during the pressing, however, remains largely speaking unaltered. This is especially true of active nickel electrodes, which are sintered at a low temperature, 500 to 600°C.

A section through the coarse layer of a working electrode is shown in Fig. 2. The powder grains are assumed to be covered by a cohesive electrolyte film. Cohesive electrolyte bridges are formed across narrow passages. The cross-sectional area is thus divided up into electrode material, film, electrolyte bridges and gas-filled spaces.

The electrode may be conceived as being a stack of sufficiently thin discs, electrode sections, which can be formed from a series of sections parallel to the electrode surface (in a homogeneous electrode material the structure of the sections is not affected by the orientation), cf. Fig. 3. The total electrode area in 1 cm^2 electrode sections available for electrochemical reaction consists of the electrode area covered by the electrolyte film, i.e., $dA = N \cdot dL \cdot s$, where N is the film length or film perimeter available, and s a tortuosity factor, the interstice tortuosity. (Electrocatalytically active material is assumed to be uniformly distributed over the electrode surface.) The area of the film covering the electrode, which can be called the film area dA, is sometimes considerably less than the actual area of the underlying electrode material.

With low differential pressures and an electrode body completely filled with electrolyte, the surface forces binding the electrolyte to the electrode material in the outer layer of the electrode exceed the gas pressure acting on the liquid body. When a certain critical pressure is reached, however, the first minute quantity of gas begins to penetrate into the electrode, see Fig. 4. The gas pressure, which acted on that part of the liquid body in the outer layer which had been forced back, then very slightly exceeds the capillary force which acted on this part of the liquid body at the instant when it was displaced. As the pressure increases, the electrolyte is displaced more and more for the same reason. The volume of the electrolyte displaced is equal to the cross-sectional area of the newly formed gas-filled spaces in a typical electrode section multiplied by the thickness, L, of the coarse layer.

An increase of dP for a differential pressure P, dyn/cm^2, results in a further gas penetration, dV, corresponding to a cross-section with an area equal to dV/L and the film perimeter dN. If the surface tension is denoted σ dyn/cm and the contact angle θ, the balance between the differential pressure and the capillary force for the elements in question gives

$$dN \cdot \sigma \cdot \cos\theta = P \cdot dV/L \qquad (1)$$

Dilatometer experiments, see below, give $V = f(P)$, from which

$$dV = f'(P) \cdot dP \qquad (2)$$

and

$$dN \cdot \sigma \cdot \cos\theta = P \cdot f'(P) \cdot dP/L \qquad (3)$$

are obtained.

Integration gives

$$N = \frac{1}{L \cdot \sigma \cdot \cos\theta} \int_0^P P \cdot f'(P) \cdot dP \qquad (4)$$

A number of significant conclusions can be drawn from Eq. (4). A high differential pressure P and a steep derivative f'(P) give a high value for N and thus a large film area for electrochemical reaction. A large film area clearly cannot be combined with a structure permitting low differential pressures, except when there is some means of altering the surface tension or contact angle.

Provided that V is an unequivocal function of P (no hysteresis), the integration, Eq. (4), can be accomplished and N is obtained as a function of P. The film area, A, is then determined with the aid of the interstice tortuosity s. Fig. 5 shows the film perimeter N as a function of the differential pressure. Since Eq. (4) has been derived on the assumption that there is no hysteresis, only the ascending curve branch in Fig. 4 has been utilised for the calculations.

The electrode activity for decreasing gas pressure often lies at a higher level than for increasing differential pressure, cf. Fig. 4. The size of the gas-filled volume per cm^2 electrode area, V, as a function of the differential pressure displays a similar hysteresis effect, which can also be seen from Fig. 4. A possible explanation of the hysteresis effect is that the electrode structure is not ideal with regard to internal communications. Certain spaces are blocked by small passages sealed with a liquid lock (the ink-stand effect). A higher gas pressure is required to open the passages and reach the blocked-off spaces.

The hysteresis effect depends partly, however, on the rate with which the process takes place. This suggests that electrolyte transport in the porous electrode is a slow process, which is not surprising in view of the large surfaces and the thin film layers.

Two different kinds of electrolyte transport can be conceived: plug flow and film flow. Plug flow would correspond to the normal flow in a pipe under the influence of a pressure gradient. This assumes that the entire cross-section in the pipe/pore is filled with liquid. The film flow would represent transport of liquid through the displacement of liquid from film regions having a higher thermodynamic potential to regions having a lower potential. Film flow compared with plug flow must be a less efficient process for material mass transfer, owing to greater frictional resistance and a low driving force. It should be possible, however, for mass transfer by means of film flow to take place independent of ink-stand structures, etc. This means that it should be possible for the hysteresis to be more or less eliminated, if the changes in pressure are made sufficiently slow to give time for the film flow. This is not contradicted by the experiments. Hysteresis is treated with the aid of an interstice model. The space between the grains in an electrode section, cf. Figs. 2 and 3, is assumed to be divided into interstices, cf. Fig. 6. These interstices are assumed to be gradually and successively filled with electrolyte as the differential pressure drops, or with gas as the differential pressure increases. This presentation is thus based on the geometrical relationships during the constriction process.

An interstice has the width D, height G and thickness equal to that, dL, of the electrode section. (D does not include the film.) The interstice thickness dL is constant and the height G is assumed to be constant so that the interstice cross-section will also be constant ($= dL \cdot G$). Under these conditions the interstice volume is consequently directly proportional to the interstice width D. Each interstice width, D, clearly corresponds to a certain differential pressure, P, which is just sufficient for gas penetration into the interstice, provided that the interstice in question can freely communicate with the gas and electrolyte side via a chain of other interstices of at least the same width.

The distribution of the interstices can be illustrated with the aid of frequency distribution curves. These can also be presented in histogram form. The associated differential pressure, P, can also be used instead of the interstice width, D, as an independent parameter in these histograms.

All interstices belonging to a given pressure class will not be filled with gas when the pressure is increased to the relevant pressure P_n under the conditions applicable to the rates of change of the pressure. To permit a simple numerical treatment of the hysteresis curve, it is assumed that a continued rise of the differential pressure to the next higher pressure class causes all interstices of the affected size not previously filled with gas now to be filled with gas. When the pressure returns to its original value, some of the interstices in question are filled with electrolyte. As a further simplification, it is assumed that all the interstices in question are filled with electrolyte again, when the pressure is reduced to the next lower pressure class.

With these assumptions it is possible to recalculate the experimentally determined hysteresis curve for the volume of the gas that has penetrated into the electrode as a function of the differential pressure to associated hysteresis curves for the film perimeter and film area. An Algol programme is utilised for the numerical treatment.

The gas penetration into the electrodes for varying differential pressure has been measured with the aid of a dilatometer, see Fig. 7. The interstice tortuosity,

s, can be determined in a conventional manner by means resistance measurements across an electrode completely filled with electrolyte in a measuring cell, see Fig. 8.

3. Structure of the electrolyte film

The area and thickness of the film are of importance to the transport of gas, e.g., hydrogen or oxygen, to the electrode surface from the gas phase right through the film to the electrode surface. Other reactants and reaction products are transported, however, in the liquid phase along the film to or from the reaction sites in the electrode surface. These transport paths run along the film covering the powder grains, and from grain to grain via electrolyte bridges and the sintered functions between the grains. This structure is called the film network, see Fig. 9. The ionic resistance of the film network and its resistance to diffusion of uncharged species depend in a similar manner on the structure. The resistance of the film network to material mass transfer can therefore be assessed through measurement of the ionic film resistance.

The available film area, A, in an electrode area of 1 cm^2 can be presented as an equivalent rectangular disc from the transport point of view with the electrode in question having a length f·L and thickness F. The transport is thus assumed to take place in the longitudinal direction.

The film tortuosity f has another significance than the interstice tortuosity, s, previously introduced. Film resistance measurements are carried out in a cell similar to that used for determining the interstice tortuosity, cf. Fig. 8. In this case, measurements are performed on electrodes provided with a fine layer on both sides of the coarse layer with the gas applied to a ring arranged around the periphery. Measurements can also be performed on normal electrodes provided with only one fine layer with the aid of a thin auxiliary fine-layer plate pressed direct on to the gas side of the test electrode.

4. Typical experimental results

Table 1 shows examples of the results obtained on different types of porous gas-diffusion electrode, but not ASEA's production electrodes.

The tortuosity factor s is utilised for determining the film area A from the film perimeter U. Values around $s = \sqrt{2}$ could be expected which corresponds to the mean value of the relationship between the surface of a plane surface element and its projection on a plane having an arbitrary slope relative to the surface element. This is in close agreement with the experimentally determined values of s according to Table 1.

The film areas for the oxygen electrodes at the maximum differential pressure in Table 1 agree fairly well with respect to order of magnitude with corresponding BET surfaces and with pore surfaces calculated from determinations on pore diameters with mercury porosimeter. As far as hydrogen electrodes are concerned, which contain nickel boride catalyst, the BET surface is considerably larger than the film area. These hydrogen electrodes clearly display a considerable atomic roughness compared with the oxygen electrode, which is also reflected in a higher value of the film thickness.

The mean value of the interstice width, $\bar{D}$, agrees rather well with the mean pore diameters determined with the mercury porosimeter, with the exception of the AMT electrode. The values of the film tortuosity, f, listed in Table 1, are very approximative owing to the inexactness of the film thicknesses determined here. When the transport properties of the film in the longitudinal direction are to be assessed, it is preferable to utilise the resistance z as a direct measure of this transport property of the film network.

Fig. 10 shows the film area as a function of the differential pressure for an oxygen electrode in 7-N KOH at 25°C. The current density at -100 mV versus Hg/HgO is plotted on the same diagram together with the film resistance. As the differential pressure increases, the current density rises in proportion to the film area, and then passes through a maximum for a further increase in the differential pressure, when the film resistance starts to become considerable. These conditions are suitable for a further simple analysis.

5. Division of electrode resistance into component terms

Limiting current density cannot be observed in technically interesting electrodes at the recommended service conditions. The current-voltage characteristic of a fuel cell during short-term runs is generally linear down to cell voltages close to zero. The apparent internal resistance in the fuel cell is thus practically speaking constant for a varying load, but with otherwise constant operating conditions, if low loads are neglected.

The internal resistance of the fuel cell can be divided up in the first place into three terms: one term associated with the ionic conductivity in the electrolyte space and the electronic conductivity in electrodes and current collectors, one term associated with the specific cathode functions and one term associated with the specific anode functions. These terms, which can each be experimentally determined are also largely speaking constant and independent of the current density, with the exception of oxygen electrodes under low load.

The apparent electrode resistance in its turn can be further divided into terms, partial resistances, having a physical significance. These partial resistances can be conceived as varying in such a way that their sum total will remain constant in agreement with experimental observations. As an alternative, the different component resistances are each constant, to the extent that they are not negligibly small compared with the total electrode resistance.

The reaction path from the gas space to the inside of the fine layer via the electrochemical reaction step in a section of an electrode is assumed to pass across three series-resistors. The first resistor can represent the resistance to gas diffusion across the film and is denoted R_g. The second resistor describes the slowness of the electrochemical reaction and is denoted R_r. The third resistor is associated with the slowness of the ion transport along the film and is denoted R_i. The reaction resistance R_r is assumed to be constant for the relevant low current densities, corresponding to a linear relationship between current density and activation polarisation. The gas-diffusion resistance, R_g, is inversely proportional, with the other conditions being constant, to the film area in the section dA and the absolute pressure p. (The film thickness F is assumed to be constant.) The ion migration resistance R_i is directly proportional to the film resistance z. The total resistance R_t can be written as

$$R_t = R_g + R_r + R_i = \frac{C_1}{dA \cdot p} + C_2 + C_3 \cdot z \qquad (5)$$

where C_1, C_2 and C_3 are assumed to be constant to the extent that the component resistances are small in relation to the total resistance. The quantities dA and z vary with the differential pressure, etc. If the electrode is assumed to be very thin, Eq. (5) may apply to the entire coarse layer, and therefore the film area A is introduced instead of dA in Eq. (5). The resistance terms R_t, R_g, R_r and R_i will then have the quantity ohm $\cdot$ cm^2 and represent weighted mean values.

Despite this considerable simplification of the actual conditions, Eq. (5) has been found to result in a qualitative agreement also with the relatively thick electrodes utilised for these measurements.

The film diffusion is the decisive factor for low film areas, and therefore the constant C_1 can be easily estimated from data for very low differential pressures. The constant C_1 is thus estimated from the plotting of the electrode resistance R_t as a function of the inverted product film area x absolute pressure, i.e., $1/(A \cdot p)$. (The electrode resistance for the hydrogen electrode has been determined through division of 0.10 V by the current density, in A/cm^2, at 0.1 V polarisation, and for the oxygen electrode by division of 0.17 V by the current density at -0.1 V versus Hg/HgO.) A straight line is drawn through the origin and points corresponding to small film areas, where the diffusion through the film is assumed to be rate-determining, Fig. 11. As a rule, the cluster of points is deflected near the Y-axis and intersects this at the ordinate, which does not lie at zero because other processes than diffusion bacome rate-determining for higher current densities. With the constant C_1 determined in this manner, $R_r + R_i = R_t - C_1/A \cdot p$ is plotted in a new diagram as a function of the film resistance z. A straight line is drawn through points associated with higher resistance values, cf. Fig. 12. This gives the constant term C_2, which is the ordinata in the origin, and the constant C_3, which is the slope coefficient for the line of regression. The constants are tested by means of calculation of current densities, which are compared with the measured values. As a rule, this gives a satisfactory relationship with a straight line across the entire range from very low current densities to high ones.

In this way it is clearly possible to divide up the apparent electrode resistance into a constant term, a term determined by the film area and a term determined by the film resistance, cf. Table 2. The constant term plays a relatively important role for the experimental electrodes and the comparatively low temperatures used during the measurements for Table 2, which implies that the electrocatalytic activity is the limiting factor in these cases. Table 2 also shows how the three component resistances vary with the differential pressure and thus how the rate-determining step depends on the differential pressure.

Table 3 lists calculated values of the electrode polarisation for the oxygen electrode type AHT at 50°C in Table 2. These calculated values agree with the measured value of 0.17 V across the entire hysteresis curve, which must be interpreted as indicating that Eq. (5), at least for this type of porous gas-diffusion electrode, effectively presents from the practical point of view the electrode resistance and its dependence on the structure parameters.

Table 1. Structure parameters for different types of fuel-cell electrodes

Type	Temp.	Differential pressure		Interstice tortuosity	Film area A	BET surface	Pore area	Mean interstice width	Mean pore diameter	Film thickness	Film resistance	Film tortuosity
	°C	Max.	Service	s	cm^2/cm^2	cm^2/cm^2	cm^2/cm^2	$\bar{D}\cdot10^{-5}$ cm	10^{-5} cm	$F\cdot10^{-5}$ cm	z ohm·cm	f
AHT (oxygen)	50	-	2.2	1.45	1000	3500	2980	8.0	7.6		29	~7
		3.4	-		2200		3900	6.3	7.1	<0.01	135	~1
-"-	25	-	2.2	1.49	860	3500	2930	8.6	7.6		23	~5
		3.4	-		2300		3900	5.9	7.1	<0.01	124	~1
ALT (oxygen)	25	-	1.2	1.69	130	2000	1150	42	15.0		52	~3
		2.6	-		1230		1740	8.1	12.5	0.02	> 358	~2
CHT (hydrogen)	25	-	3.0	1.31	1370	15000	2340	5.9	5.1		74	~8
		3.4	-		2430			5.9		0.5	~100	~5
CHT (hydrogen)	25	-	2.0	1.49	630	15300	1360	10	7.9		39	~8
		3.4	-		1250		1980	8.3	7.2	0.8	103	~6

Table 2. Calculated partial resistances for different types of fuel-cell electrodes as a function of the differential pressure (ascending branch of the hysteresis curve).

Type	Temp. °C	C_1 x 10^{-8} ohm·dyn	C_2 ohm·cm^2	C_3 cm	Differential pressure P · 10^{-6} dyn/cm^2	Film area A cm^2/cm^2	Film resistance z ohm · cm	Calculated resistance values R_g ohm·cm^2	R_r ohm·cm^2	R_i ohm·cm^2	R_t ohm·cm^2
AHT (oxygen)	50	2.4	0.85	0.0086	1.0	23	6.1	4.3	0.85	0.05	5.2
					1.8	450	9.2	0.18	0.85	0.08	1.1
					2.2	1000	29	0.07	0.85	0.25	1.2
-"-	25	7.4	1.7	0.023	1.0	13	8.3	29	1.7	0.19	31
					1.8	280	10.2	0.94	1.7	0.23	2.9
					2.2	860	23	0.27	1.7	0.53	3.5
AMT (oxygen)	25	2.8	4.3	0.0098	1.0	25	20	5.6	4.3	0.20	10
					1.2	130	52	0.98	4.3	0.51	5.8
					2.0	1000	360	0.09	4.3	3.5	7.9
CHT (hydrogen)	25	20	2.5	0.0038	1.0	10	8.5	100	2.5	0.03	103
					1.8	14	9.4	51	2.5	0.04	54
					3.0	1370	74	0.36	2.5	0.28	3.1
CMT (hydrogen)	25	1.2	2.0	0.023	1.0	40	8.2	1.5	2.0	0.19	3.7
					1.6	290	25	0.16	2.0	0.57	2.7
					2.0	630	39	0.06	2.0	0.90	3.0

Table 3. Calculated electrode polarisation for experimental electrode type AHT at 50°C (cf. Tables 1 and 2)

Differential pressure P · 10^{-6} dyn/cm^2	Direction of pressure change	Film area A cm^2/cm^2	Film resistance z ohm · cm^2	Calculated resistance R_t ohm · cm^2	Current density at 0.17 V polarisation I A/cm^2	Calculated polarisation V
1.0	up	28	6.1	5.2	0.039	0.20
1.8	"	450	9.2	1.1	0.123	0.14
2.6	"	1440	61	1.4	0.111	0.16
3.4	max.	2200	137	2.0	0.081	0.16
2.6	down	1970	95	1.7	0.108	0.18
1.8	"	1070	52	1.4	0.132	0.18
1.0	"	110	18	2.1	0.095	0.20

References

1. Lindström, O., Teknisk Tidskrift 93, 593 (1963).

2. Lindström, O., ASEA Journal 37, 3 (1964).

3. Will, F.G., J. Electrochemical Soc. 110, 145 (1963).

4. Will, F.G., J. Electrochemical Soc. 110, 152 (1963.

5. Ksenzhek, O.S., in Bagotskii, V.S. and Vasilév, Y.B., "Fuel Cells", Consultants Bureau, New York, 1966, p. 1.

6. Micka, K., Collection Czech. Chem. Commun. 29, 1998 (1964).

7. Newman, J.S. and Tobias, Ch.W., Electrochem. Soc. 109, 1183 (1962).

8. Lindström, O., ASEA Journal 40, 91 (1967).

9. Lindström, O., Entropie 14, 58 (1967).

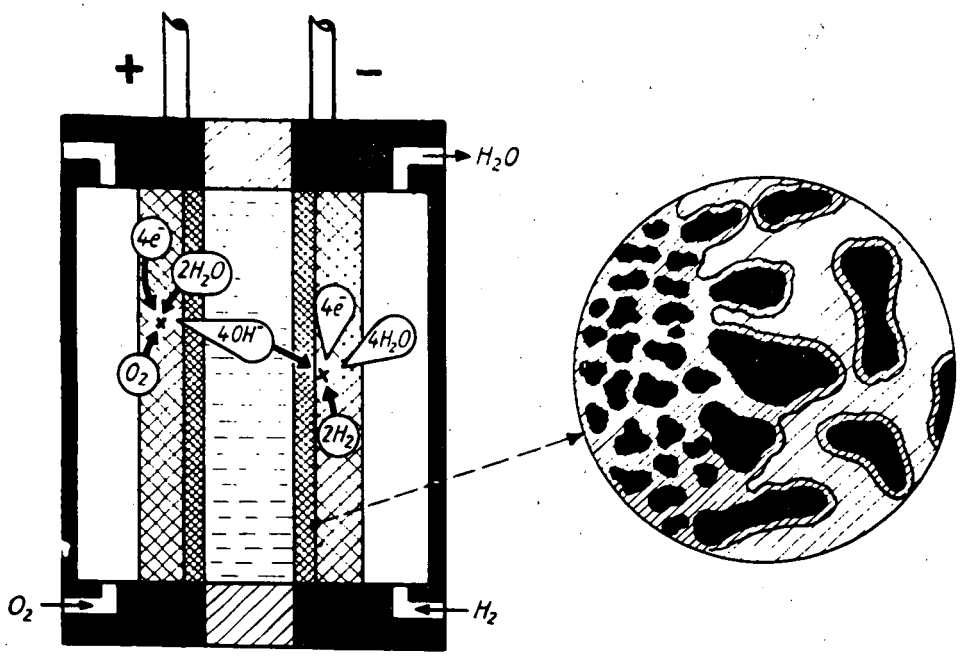

Fig.1. Electrolyte film in a porous gas-diffusion electrode (from references 1 and 2)

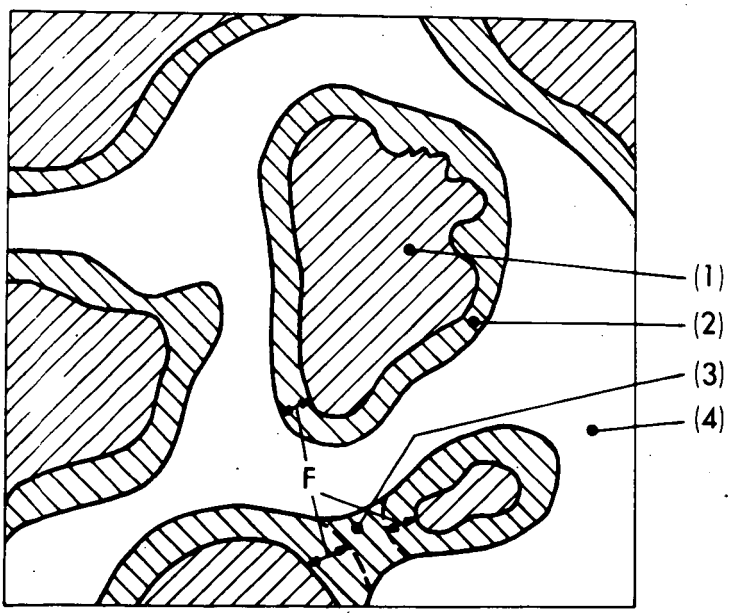

Fig.2. Section through the coarse layer of a working electrode

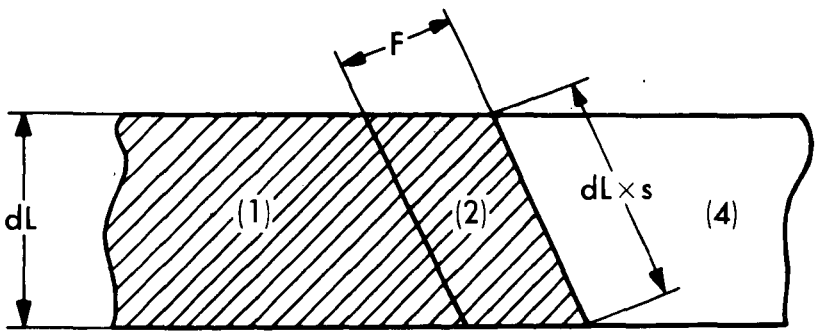

Fig. 3. The electrode section viewed from the side (for the notation see Fig. 2)

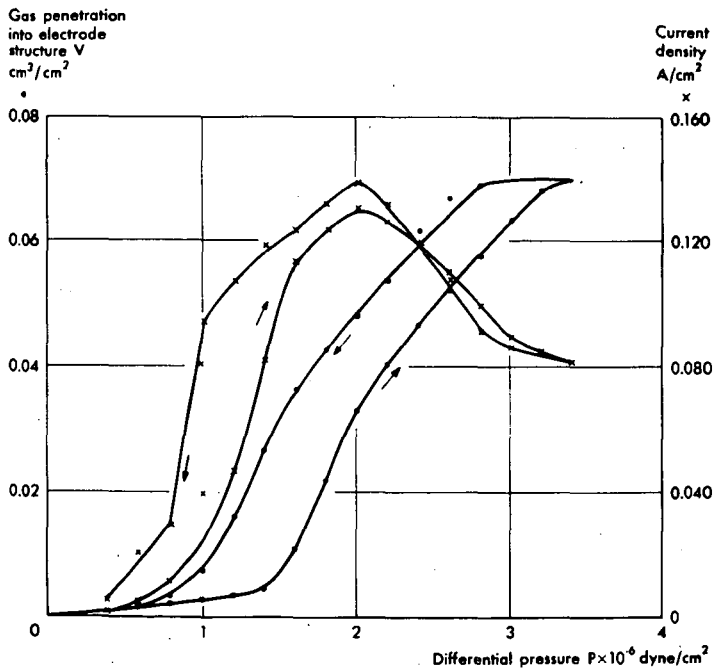

Fig. 4. Gas penetration into a hydrogen electrode, given as cm^3 gas/cm^2 electrode (V), and electrochemical activity, given as A/cm^2 at 800 mV versus Hg/HgO, as a function of the differential pressure P, dyn/cm^2

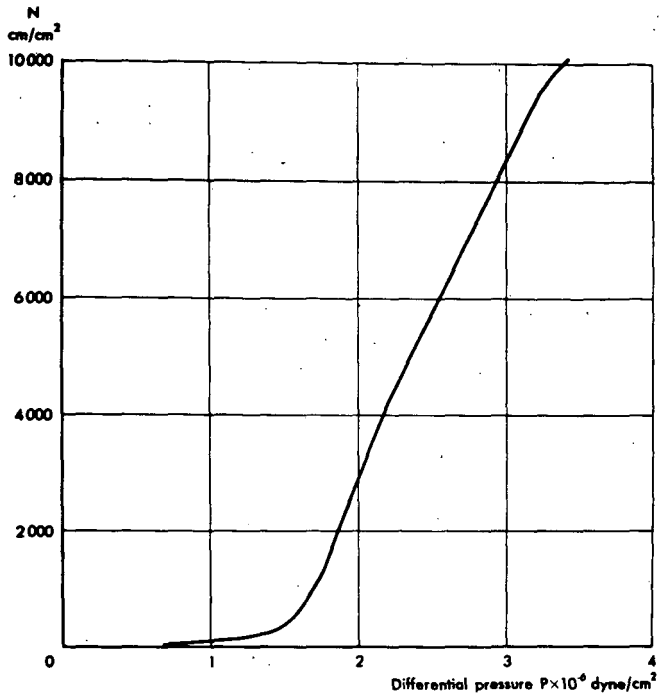

Fig. 5. The film perimeter N, cm/cm^2 electrode, as a function of the differential pressure P, dyn/cm^2

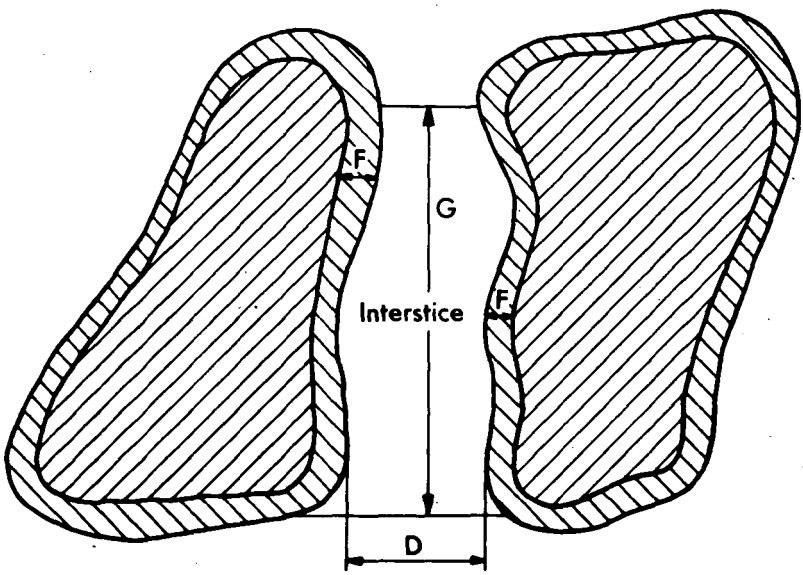

Fig. 6. Interstice model for the treatment of electrolyte penetration

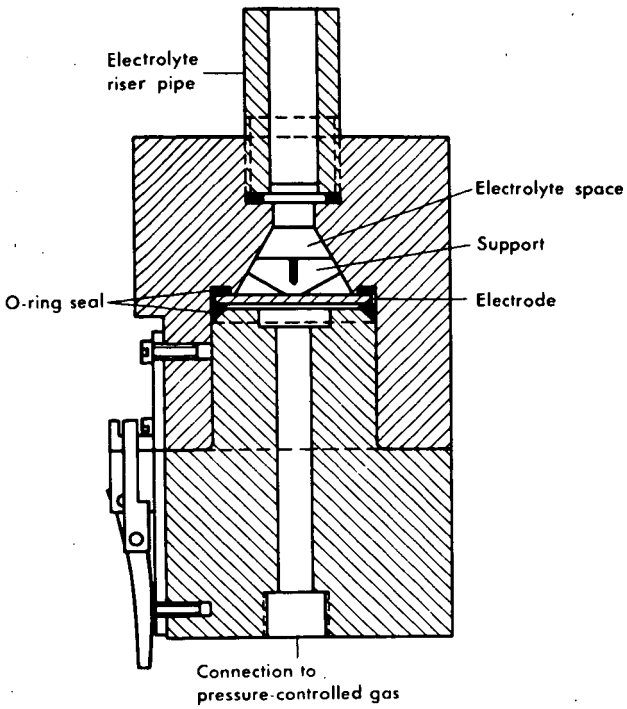

Fig. 7. Dilatometer for measuring the gas penetration into porous gas-diffusion electrode

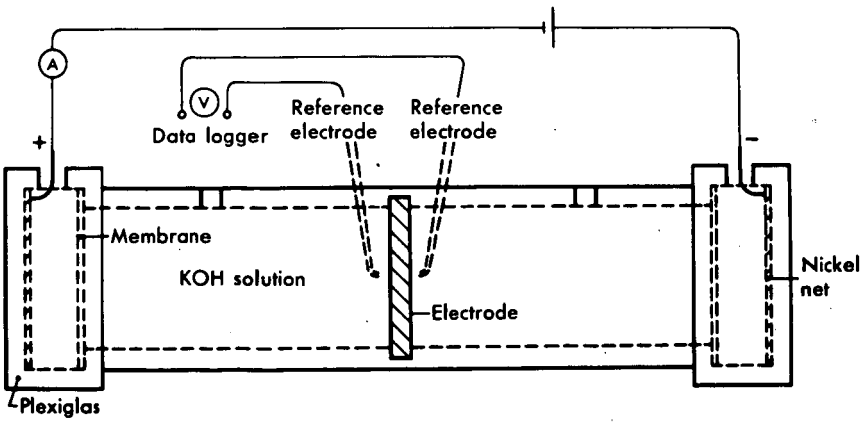

Fig. 8. Arrangement for determining the electrolyte resistance in fuel-cell electrodes

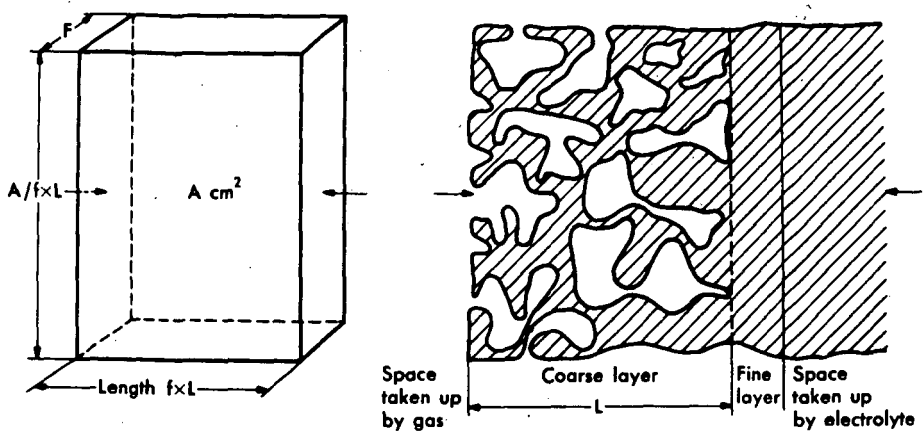

Fig. 9. Model of the film network and the equivalent disc

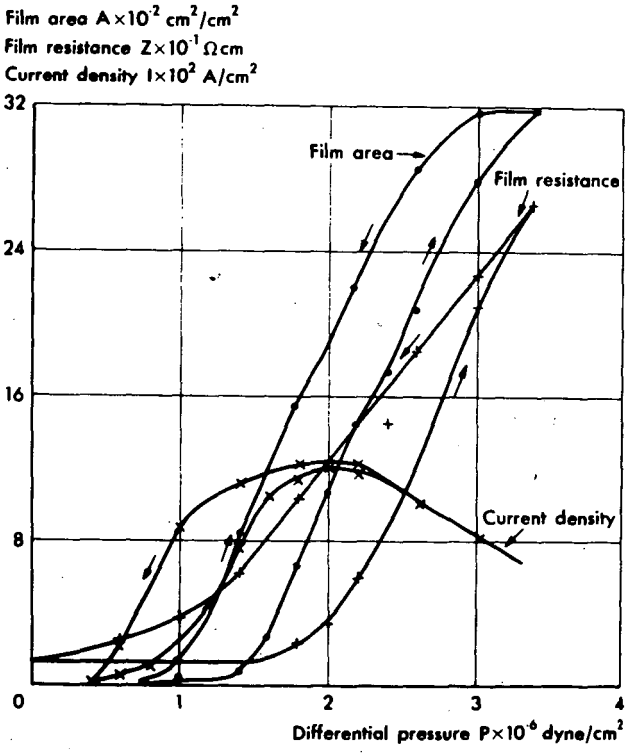

Fig. 10. Film area A, cm^2/cm^2 electrode, film registance z, ohm · cm, and electrode activity, mA/cm^2 at −100 mV versus Hg/HgO, as a function of the differential pressure P, dyn/cm^2, for an oxygen electrode in 7-N KOH at 25°C

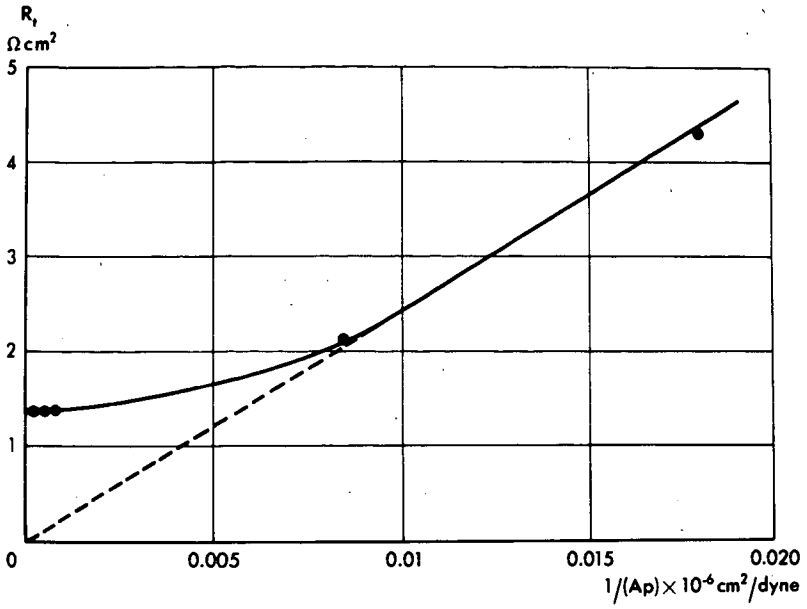

Fig. 11. Estimation of the constant C_1 in Eq. (5)

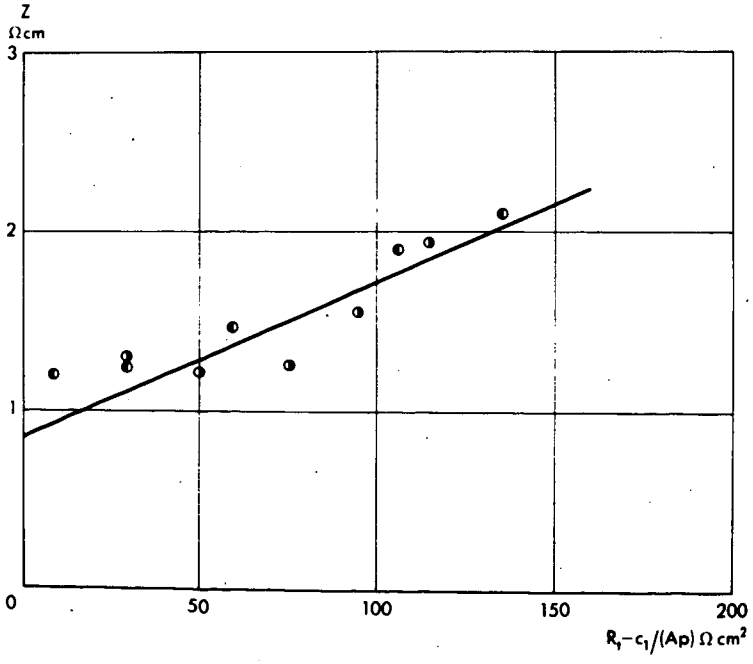

Fig. 12. Estimation of the constants C_2 and C_3 in Eq. (18)